Author Manuscript

Author Manuscript

Author Manuscript

Author Manuscript

HHS Public Access

Author manuscript

Chemistry. Author manuscript; available in PMC 2015 July 09.

Published in final edited form as:

Chemistry. 2012 December 14; 18(51): 16349–16357. doi:10.1002/chem.201202072.

IR-Monitored Photolysis of CO-Inhibited Nitrogenase: A Major EPR-Silent Species with Coupled Terminal CO Ligands

Lifen Yan[a], **Dr. Vladimir Pelmenschikov**[b], **Christie H. Dapper**[c], **Aubrey D. Scott**[a], **Prof. William E. Newton**[c], and **Prof. Stephen P. Cramer**[a,d]

Vladimir Pelmenschikov: pelmentschikov@mailbox.tu-berlin.de; Stephen P. Cramer: spjcramer@ucdavis.edu

[a]Department of Chemistry, University of California, Davis, CA 95616

[b]Institut für Chemie, Technische Universität Berlin, 10623 Berlin, Germany

[c]Department of Biochemistry, Virginia Polytechnic Institute, Blacksburg, VA 24061, USA

[d]Physical Biosciences Division, Lawrence Berkeley National Lab, Berkeley, CA 94720

Abstract

We have used Fourier transform infrared spectroscopy (FT-IR) to observe the photolysis and recombination of a novel EPR-silent CO-inhibited form of α-H195Q nitrogenase from *Azotobacter vinelandii*. Photolysis at 4 K yields a strong negative IR difference band at 1938 cm^{-1}, along with a weaker negative feature at 1911 cm^{-1}. These bands and the associated chemical species have both been assigned the label 'Hi-3'. A positive band at 1921 cm^{-1} is assigned to the 'Lo-3' photoproduct. By using an isotopic mixture of $^{12}C^{16}O$ and $^{13}C^{18}O$, we show that the Hi-3 bands arise from coupling of two similar CO oscillators with one uncoupled frequency at ~1917 cm^{-1}. Although in previous studies Lo-3 was not observed to recombine, by extending the observation range to 200–240 K we found that recombination to Hi-3 does indeed occur, with an activation energy of ~6.5 kJ mol^{-1}.

The frequencies of the Hi-3 bands suggest terminal CO ligation. We tested this hypothesis with DFT calculations on models with terminal CO ligands on Fe2 and Fe6 of the FeMo-cofactor. An $S = 0$ model with both CO ligands in *exo* positions predicts symmetric and asymmetric stretches at 1938 and 1909 cm^{-1} respectively, with relative band intensities of ~3.5:1, in good agreement with experiment. From the observed IR intensities, we find that Hi-3 is present at a concentration about equal to that of the EPR-active Hi-1 species. The relevance of Hi-3 to the nitrogenase catalytic mechanism and its recently discovered Fischer-Tropsch chemistry is discussed.

Keywords

nitrogenase; Fischer-Tropsch; photolysis; CO; DFT

Correspondence to: Vladimir Pelmenschikov, pelmentschikov@mailbox.tu-berlin.de; Stephen P. Cramer, spjcramer@ucdavis.eduspcramer@lbl.gov.

Supporting information for this article is available on the WWW under http://www.chemeurj.org/ or from the author.

Author Manuscript Author Manuscript Author Manuscript Author Manuscript

Introduction

The enzymatic nitrogen fixation system known as nitrogenase (N_2ase) catalyzes the reduction of dinitrogen to ammonia at ambient temperatures and atmospheric pressure.[1] For the Mo-dependent N_2ase, binding of substrates and inhibitors involves a [Mo-7Fe-9S-**X**]-homocitrate-containing prosthetic group, called the FeMo-cofactor, of the larger MoFe protein (*Av1*). A recent crystal structure at 1.0 Å resolution[2] and an X-ray emission study[3] favor assigning C^{4-} carbide as the much-debated atom **X** at the center of the cofactor. The mechanism by which this biological nanoparticle lowers the activation energy for reduction of the N≡N triple bond remains incompletely understood.

Carbon monoxide inhibits the reduction of N_2 reversibly and non-competitively, and CO has been an important probe molecule for characterizing the active site.[4] Recently, Ribbe and coworkers have shown that CO can actually be a substrate for the V version of N_2ase,[5] and with less efficiency, even for the wild-type Mo-dependent N_2ase.[6] Seefeldt and coworkers have also demonstrated CO fixation, using the *α*-V70A and other variants of the MoFe protein.[7] Thus, a second front of interest in N_2ase as a Fischer-Tropsch catalyst has emerged.[8]

Exposure of N_2ase to CO during turnover elicits species with a variety of EPR signals, depending on the partial pressure of CO ([CO]), and each of these species and its characteristic EPR signal is described by the [CO] required for its formation.[9] The chemical species and its associated axial EPR signal (*g*-values near 2.17 and 2.06) are both called hi-CO and are formed under ~101 kPa [CO]. This hi-CO N_2ase species is proposed to contain two CO molecules bound to the FeMo-cofactor.[9–10] A species with a rhombic EPR spectrum (*g*-values of 2.09, 1.98, and 1.93) called lo-CO forms under a much lower [CO][11] and is proposed to contain only one bound CO.[9–10] A third species and EPR signal, both called hi(5)-CO, have also been identified.[11c, 11d] Not all of these EPR signals are generated when variant Mo N_2ases are turned over under CO,[12] and the integrated EPR intensities rarely exceed 40% of the active site species.[11d] Presumably, EPR-silent species with bound CO must co-exist with the EPR-active species.

Another spectroscopic tool that complements EPR for these studies has been FT-IR spectroscopy.[4c, 13] In stopped flow FT-IR experiments, under low [CO], a single ν(CO) band appeared at 1904 cm^{-1} and peaked in intensity within ~7s before decaying. Under high [CO], a new ν(CO) band was observed at 1936 cm^{-1} together with a pair of weaker, possibly coupled bands at 1958 and 1880 cm^{-1}. All of these features were much longer lived than the 1904 cm^{-1} band. All three species were suggested to arise from terminally bound CO. After relatively long times (>10s), under low [CO] the 1904 cm^{-1} peak is succeeded by a new ν(CO) band at 1715 cm^{-1}. Recently, the rates and relative intensities of these ν(CO) bands were shown to be sensitive to variation of the side-chain at the *α*-70 position.[13c] Other CO-related IR bands have been observed during spectro-electrochemical studies of FeMoco (the solvent-extracted version of the FeMo-cofactor),[14] where bands at 1808 and 1835 cm^{-1} were proposed to arise from bridging CO, whereas features at 1885 and 1920 cm^{-1} were assigned to terminally bound CO species.

Author Manuscript Author Manuscript Author Manuscript Author Manuscript

In a recent study of CO-inhibited *Azotobacter vinelandii* Mo nitrogenase, we showed that FT-IR can be used to monitor CO photolysis by visible light at cryogenic temperatures.[15] Three distinct types of photolyzable CO complexes were found under hi-CO conditions. We labeled these stable inhibited forms 'Hi-1', 'Hi-2', and 'Hi-3'. The photolyses of Hi-1 and Hi-2 were found to be reversible at around 80 K, with activation energies on the order of 3–4 kJ mol^{-1}. However, the Hi-3 photoproduct, labeled 'Lo-3', was stable with respect to recombination up to 110 K. The Hi-3 species was most abundant in the photolysis spectra of N_2ase with the variant α-H195Q MoFe protein. In the current work, we have used this variant and an extended temperature range (~200–250 K) to discover that Hi-3 photolysis is also reversible. We have used mixed CO isotopes to demonstrate vibrational coupling in the Hi-3 species, and wavelength-dependent photolysis to determine the spectral region with the greatest photochemical activity. We have also estimated the relative amounts of the Hi-1 and Hi-3 species in our samples. Finally, we have employed DFT calculations to evaluate plausible structures for Hi-3 and Lo-3 CO-bound FeMo-cofactor species.

Results

Photolysis

Figure 1 shows the time courses of changes in the IR spectra of CO-inhibited α-H195Q N_2ase samples illuminated with visible light at ~4 K under either $^{12}C^{16}O$ or $^{13}C^{18}O$. Photolysis spectra under $^{13}C^{16}O$ are included in Figure 2. At long times, the largest spectral changes come from the Hi-3 species,[15] with a strong negative band at 1938 (1894, 1849) cm^{-1} and a weaker negative band at 1911 (1867, 1824) cm^{-1}. A positive product band from Lo-3 is seen in between these two bands at 1921 (1877, 1833) cm^{-1}. (In these and later descriptions, the first value refers to results with $^{12}C^{16}O$ whereas the second and third values in parentheses, if present, refer to results with $^{13}C^{16}O$ and $^{13}C^{18}O$, respectively.) As noted before[15], for α-H195Q N_2ase the spectra are complicated by the presence of other photolyzable species, including bands for Hi-1 at 1969 (1925, 1879) cm^{-1} and for Hi-2 at 1932 (1888, 1844) cm^{-1}.

The spectra can be simplified by employing the fact that the photolysis product Lo-3 is relatively stable at temperatures where the photolysis products from Hi-1 and Hi-2 rapidly recombine.[15] Accordingly, we warmed the photolyzed samples to 120 K for 10–20 min and then photolyzed a second time. As shown in Figure 1, there was almost no trace of the Hi-3 or Lo-3 features in the second photolysis spectrum, consistent with the absence of Hi-3. By taking the difference between the two photolysis results, we obtained a relatively pure Hi-3→Lo-3 photolysis signal in the double difference spectrum (Figure 2). The extracted spectrum exhibited almost pure Hi-3 features at the same frequencies as noted in the mixed spectra. Note that in the third photolysis spectrum, which followed warming the sample from the second photolysis to above 230 K, the Hi-3→Lo-3 signals reappeared.

An alternative method of cleanly separating the Hi-3 features is to photolyze at higher temperatures, where the recombination of the other photolysis products is fast. As shown in Figure 2, photolysis of a $^{13}C^{16}O$ sample at 240 K yielded a spectrum with a pair of negative bands at 1891 and 1864 cm^{-1}; nearly the same as the frequencies (1894 and 1867 cm^{-1}) seen in the low-temperature photolysis. In fact, the 3 cm^{-1} downshifts are similar to those

Author Manuscript Author Manuscript Author Manuscript Author Manuscript

seen in myoglobin-CO upon raising the temperature from 4 K to room temperature.[16] This observation suggests that we should anticipate comparable shifts between our liquid helium-temperature photolysis results and the room-temperature stopped-flow FT-IR studies. In these higher temperature photolyses, there was less evidence of the Lo-3 photolysis product. We cannot exclude the possibility that additional processes involving CO migration and rearrangement and/or possible Lo-3 photolysis might be occurring at higher temperatures; these issues call for additional study.

Recombination

As seen in Figure 2, Hi-3 returns on the 1h time scale upon warming the sample to ~210 K. From monitoring this process at various temperatures, Arrhenius plot analysis using the initial rates yields an activation energy of ~6.5 kJ mol^{-1} (Figure 2), compared to the ~4 kJ mol^{-1} values previously seen for Hi-1 and Hi-2 recombination.[15] (In more recent studies we have found that with brief irradiation, the Hi-2 recombination can occur with a much smaller activation energy).[17] The Hi-3 value is similar to the barriers of 8–10 kJ mol^{-1} seen for Ni-SI_a→NiSCO CO recombination in [NiFe] hydrogenases[18] and for photolyzed MbCO.[19]

Mixed Isotope Studies

The relative intensities of the negative Hi-3→Lo-3 features involve a higher 1938 (1894, 1849) cm^{-1} frequency band that is about four-times stronger than its lower 1911 (1867, 1824) cm^{-1} frequency partner. One explanation for the different intensities of the high and low frequency bands is that they represent the symmetric (with I_{sym} intensity) and antisymmetric (I_{asym}) combinations of stretches for two distinct terminally bound CO molecules. Assuming that the symmetric combination has the higher frequency, the equation $I_{sym}/I_{asym} = \cot^2\theta$ where θ is half the angle between the CO molecular axes, can be used to calculate a rough approximation of the relative orientations of the two molecules[20]. For an intensity ratio of ~4, the angle 2θ between CO axes is predicted to be ~50°. Such an angle is too small for two CO molecules bound at the same metal ion. Furthermore, coupling of vicinal $^{12}C^{16}O$ molecules usually produces splittings of about ~40–60 cm^{-1},[20] approximately twice as large as that observed for Hi-3. Both observations support the notion that there are two vibrationally coupled CO ligands, each of which is bound to a *different* FeMo-cofactor metal ion.

To confirm the assignment of the Hi-3 signals to coupled oscillators, we recorded photolysis spectra for α-H195Q N_2ase inhibited by a mixture of ~25% $^{12}C^{16}O$ and ~75% $^{13}C^{18}O$. In the absence of coupling, such a sample would produce a spectrum that is the 25:75 = 1:3 weighted average of the two pure 100% $^{12}C^{16}O$ and 100% $^{13}C^{18}O$ spectra, respectively. However, as seen in Figure 3, the mixed-CO spectrum has a new negative band at 1917 cm^{-1}. This band does not appear in the 2nd photolysis spectrum after recombination at 120 K (see Figure 1 for the reference), so we can rule out assigning it to either Hi-1 or Hi-2. As expected for a Hi-3 assignment, the 1917 cm^{-1} band does reappear in the 3rd time photolysis, after recombination overnight at 233 K. We interpret this new band as resulting from photolysis of a Hi-3 species involving uncoupled CO oscillators, one with $^{12}C^{16}O$ and

Author Manuscript Author Manuscript Author Manuscript Author Manuscript

the other with $^{13}C^{18}O$. Thus, at least one of the CO ligands is predicted to have an uncoupled frequency of 1917 cm^{-1}.

Wavelength-Dependent Photolysis

So far, we have identified three forms of CO-inhibited N_2ase that are produced under high [CO] conditions and are photolyzed by exposure to white light. To better distinguish these species, we investigated the wavelength dependence of the photolysis rates, and the results of these studies are shown in Figure 3. The Hi-3 photolysis rate rises from near zero at 600 nm to maximum efficiency at 340 nm, the shortest wavelength investigated. There appear to be minor features at ~550 and ~400 nm. By comparison, the Hi-1 species, which we associate with the hi-CO EPR species previously examined by Maskos and Hales, exhibits a structureless rise in photolysis efficiency towards shorter wavelengths. For Hi-1, we did not see the minor peak in photolysis yield at ~550 nm that was observed in the previous EPR experiments.[21]

DFT Calculations

To put speculation about the structure of the Hi-3 species on firmer ground, we used DFT calculations to investigate models that involve pairs of terminal CO ligands on different FeMo-cofactor metal sites. With 8 metal ions, there are 8(8−1)/2 = 28 possible pairs of binding sites on this prosthetic group. For the current study, we limited the calculations to binding at the most commonly proposed sites, the Fe2 and Fe6 ions on the face adjacent to the *α*-V70 residue.[13c, 22], see Figure 4. The atom and residue numbering here are as in the crystal structure.[23].As done in a recent study by Dance,[24] we considered *exo* (CO *trans* to the central **X** atom, now known to be carbon) and *endo* (CO *trans* to μ^3 sulfurs, S1A/S1B when coordinated at Fe2/Fe6, respectively) terminal binding modes, which are subsequently referred as "Fe2/Fe6 *exo*/*endo*" geometries. A less popular bridging binding mode,[25] where the CO carbon occupies a position similar to that of μ^2 S2B sulfur, was also considered. Below, we will discuss mostly those CO coordinations that were found relevant in context of the Hi-3 and Lo-3 photolytic species; a detailed description of the binding alternatives will be covered separately.

Our favored model for Hi-3 is shown in Figure 4. In the DFT calculation we assumed an EPR silent state for the transition metal ion core of the FeMo-cofactor, $1e^-$ reduced from the $S = 3/2$ resting state. Other details on the metal oxidation states and spin coupling are given in the Discussion section. In line with earlier modelling by us and many others,[26] the central ligand **X** was initially assigned as N^{3-}. Subsequently, as described below, we considered the **X** = C^{4-} alternative which has recently received significant support.[2–3, 27] The μ^2 S2B sulfur that bridges Fe2 and Fe6 and forms the hydrogen bond to *α*-H195 in the wild-type enzyme was chosen as the protonation site for all the models. Terminal CO ligands are at Fe2 and Fe6, both in the *exo* geometry, and the Fe-C≡O bond angles are essentially 180° (Figure 4). This model predicts two coupled $^{12}C^{16}O$ stretching modes, a symmetric stretch at 1938 cm^{-1} and an asymmetric stretch at 1909 cm^{-1}, with relative band intensities of ~3.5:1, in good agreement with the experimental frequencies of 1938 and 1911 cm^{-1} and amplitude ratio of ~3.7:1. (Here and below, the broadened peak center heights are compared relative to the FT-IR, see Figure 5, in contrast to the raw 'stick' DFT mode

Author Manuscript Author Manuscript Author Manuscript Author Manuscript

intensities in Table S2 of the Supporting Information.) The optimized angle between the bound CO molecular axes is 37°, in line with the above ~50° rough estimate based on the relative FT-IR Hi-3 intensities. The basic FeMo-cofactor framework remained intact. However, we note a significant lengthening of the Fe6-**X** bond to 2.17 Å, compared to an average of 2.00 Å for the remaining optimized central Fe-**X** distances. The plasticity of the FeMo-cofactor core has been observed in other calculations; where even a complete loss of Fe coordination to **X** (Fe-**X** > 3.0 Å) upon ligand binding has been predicted.[24, 26c]

For the Lo-3 photolysis product, the structure with the best match to the FT-IR Lo-3 band at 1921 cm^{-1} involved Fe2 *exo* binding (Figure 4), producing a $^{12}C^{16}O$ frequency at 1923 cm^{-1}. The calculated band intensity of this ν(CO) stretch is ~2.1:1 relative to the asymmetric Hi-3 mode at 1909 cm^{-1}, in reasonable agreement with the ~1.7:1 ratio seen in the experiment (Figure 2). For photolysis conducted using the pure $^{13}C^{18}O$ isotope, the DFT results are essentially of the same quality as those described above for $^{12}C^{16}O$.

The calculations also shed light on our mixed isotope experiments. For models with $^{12}C^{16}O$ at Fe2 *exo* or Fe6 *exo* positions (and the other Fe site populated by $^{13}C^{18}O$), they predict essentially 'uncoupled' pairs of ν(CO) frequencies of 1934/1825 or 1916/1842 cm^{-1} respectively, see the Supporting Information for the animated vibrational modes. We also modeled the actual Hi-3→Lo-3 photolysis IR spectra for 100% $^{12}C^{16}O$, 100% $^{13}C^{18}O$, and mixed isotope ~25% $^{12}C^{16}O$ / ~75% $^{13}C^{18}O$ experiments using our DFT frequency and intensity predictions, see Table S1 in the Supporting Material for the details. Figure 5 shows that in the low frequency 1810–1860 cm^{-1} region, the mixed isotope spectrum is dominated by the $^{13}C^{18}O/^{13}C^{18}O$ contributions, and the decoupled $^{13}C^{18}O$ bands are obscured by these features. However, in the higher 1900–1950 cm^{-1} frequency region, the mixed isotope species provides most of the intensity, and the DFT peaks at 1934 and 1916 cm^{-1} show noticeable shifts (of −4 and +7 cm^{-1}) with respect to the pure $^{12}C^{16}O$ isotope Hi-3 features. The FT-IR bands seen at 1934 and 1917 cm^{-1} can now be assigned to essentially uncoupled stretching modes of the $^{12}C^{16}O$ at Fe2 and Fe6 respectively, when $^{13}C^{18}O$ binds at the other Fe site. The kinetic energy distribution (KED) factors in Table S2 of the Supporting Material indicate that less than 2% energy is accumulated in $^{13}C^{18}O$ stretch in these modes, and $^{12}C^{16}O$ stretch accounts for the rest.

As mentioned above, we also considered models with the same CO binding modes and with the now-favored **X** = C^{4-} as the central ligand of the FeMo-cofactor. With the same μ^2 S2B-H protonation scheme as for the **X** = N^{3-} case, the calculations yielded bound ν(CO) frequencies >30 cm^{-1} red-shifted compared to the observed FT-IR values and optimized structures qualitatively identical to those presented in Figure 4. An extra proton addition at the μ^2 S5A FeMo-cofactor sulfur places our **X** = C^{4-} model at the same charge level (−3 units) as that of the **X** = N^{3-} model, and it significantly improves the correspondence with the FT-IR experiment. For the calculated Hi-3 ($^{12}C^{16}O$ and $^{13}C^{18}O$) ν(CO) modes, the consistent negative deviation from the FT-IR peaks is 6–8 cm^{-1}, while for the Lo-3 modes it is positive 2–3 cm^{-1}, see Table S2 and S3 of the Supporting Material.

Author Manuscript Author Manuscript Author Manuscript Author Manuscript

Discussion

Studies of the interaction of CO with N_2ase have a long history dating back to at least 1941.[4a] The subject has taken on added significance with the discovery of N_2ase Fischer-Tropsch-like CO reduction and condensation chemistry.[5–8] To date, nearly all the discussion about the structure and reactivity of CO intermediates has centered about two EPR-observable species, hi-CO and lo-CO.[9–10, 28] However, since integration of these EPR signals usually accounts for less than 50% of the enzyme, it is obvious that a good deal (50% or more) of N_2ase-CO chemistry has not been accounted for.

To access these EPR/ENDOR-silent species, we have employed an FT-IR-monitored photolysis technique in much the same way as used in myoglobin-CO studies.[29] Our initial results[15] under high [CO] conditions indicated the presence of a previously unrecognized species that we labelled Hi-3, which was EPR-silent and so did not correlate with any of the known EPR-active species. In this current study, we have elucidated the spectroscopic properties, photochemistry, and likely structures of Hi-3 and its photolysis product Lo-3. As part of assessing the significance of these new EPR-silent species, an obvious question is: what fraction of our N_2ase samples is present in these forms?

We can estimate Hi-3 abundance relative to Hi-1, by assuming (*i*) that Hi-1 contains a *single terminal* CO (as well as a second either bridging and/or more reduced CO species) bound at the FeMo-cofactor and (*ii*) that the sum of the oscillator strengths of the Hi-3 signals at 1938 and 1911 cm^{-1} (from *two coupled* CO oscillators) corresponds to twice the strength of the Hi-1 signal at 1969 cm^{-1} (from a *single* CO). From integrating the intensities of bands shown in Figure 1, the Hi-3 population is estimated as ~95% that of Hi-1. Although this is only an estimate, it is clear that the Hi-3 species is a major component of the reaction mixture. From the same assumptions, Hi-1 and Hi-3 signal concentrations are both significantly higher than that of Hi-2. Previous integrations of the EPR spectra of the α-H195Q MoFe protein under high [CO] conditions found 26% hi-CO, 6% hi(5)-CO, and 8% resting state enzyme.[11d] In some of our samples the hi-CO signal approaches 50% of the total MoFe protein. Thus, if we make the further assumption (*iii*) that the Hi-1 IR species is the same as the hi-CO EPR species,[15] then we conclude that at least a quarter and sometimes approaching half of our samples is present as Hi-3.

The combination of IR-detected photolysis experiments and DFT calculations has allowed us to propose a model for the Hi-3 species that involves two terminal *exo* CO ligands, one bound to each of the adjacent Fe2 and Fe6 sites of the FeMo-cofactor that are bridged by the protonated μ^2 S2B sulfur (see Figure 4). Vibrational coupling between these two terminal CO molecules is proposed to contribute to the ~27 cm^{-1} frequency splitting and helps explain relative ~3.7:1 intensities of the Hi-3 bands at 1938 and 1911 cm^{-1}. In the present study, such coupling was confirmed by the appearance of a new band at 1917 cm^{-1} in samples inhibited by a mixture of $^{12}C^{16}O$ and $^{13}C^{18}O$ isotopes. Our DFT model for Hi-3 lends support to this proposal. The model yields a 29 cm^{-1} splitting and relative intensities of ~3.5:1 for the coupled ν(CO) modes, symmetric at 1938 cm^{-1} *vs.* asymmetric at 1909 cm^{-1}. The long-range vibrational coupling between CO molecules bound at the Fe sites ~2.7 Å apart can be rationalized by (*i*) approximate symmetry of the proposed Hi-3 structure with

Author Manuscript Author Manuscript Author Manuscript Author Manuscript

respect to the plane formed by the three μ^2 S sulfurs (and the central **X** ligand), and (*ii*) electronic delocalization inherent to the iron-sulfur clusters such as FeMo-cofactor. Notably, this vibrational coupling may have implications to Hi-3 reactivity. Although our structural model is similar to one proposed by Hoffman and coworkers to account for properties of the hi-CO EPR signal,[10, 28b] we instead are using it to account for the properties of an EPR-silent species. Our prior results for the Hi-1 IR species, which we equate with the hi-CO EPR species,[15] indicate that this form instead has a single terminal CO with perhaps either a bridging CO or formyl ligand.

Dance has also conducted DFT calculations on CO-inhibited FeMo-cofactor with adjacent terminal CO ligands.[24] Two of his models (designated **10** and **11**) with Fe2 *exo* and Fe6 *exo* CO ligands (for the resting state $S = 1/2$ cofactor, no protons added, and using $\mathbf{X} = N^{3-}$) most closely correspond to our current Hi-3 DFT proposal and carry the same total negative charge of $3e^-$. These models, which differ only by 'coordinative allosterism' in bonding with the central atom **X**, are predicted to have somewhat lower ν(CO) frequencies of 1914/1886 and 1904/1893 cm^{-1} for **10** and **11**, respectively, than the 1938/1911 cm^{-1} pair observed in our experiments, and the intensity ratios were less than 2:1. From the present experience, these shifts could possibly be brought in line with our IR and DFT results *via* addition of one electron, and one proton at μ^2 S sulfur. The importance of the electron and proton count for the bound ν(CO) frequencies and other FeMo-cofactor properties is also outlined below.

For the Lo-3 photolysis product, our favored DFT-based model places a single CO ligand in the Fe2 *exo* position (see Figure 4), implying that the net result of photolysis is displacement of the CO ligand from Fe6. We cannot exclude the possibility that photolysis of CO from the Fe2 position also occurs, with subsequent relaxation to the preferred structure. The DFT model yields a calculated ν(CO) band at 1923 cm^{-1}, which compares well with the Lo-3 FT-IR signature at 1921 cm^{-1}. The calculated intensity of this band is ~2.1:1 relative to the lower frequency Hi-3 mode, compared to the ~1.7:1 ratio seen in the FT-IR experiment. Dance also modeled FeMo-cofactor structures with only one CO ligand.[24] Most relevant to our proposed Lo-3 structure is his model **8**, which places CO at Fe2 *endo* and yields a calculated ν(CO) frequency of 1904 cm^{-1}. Other models with Fe2-H and/or Fe6-H hydrides in addition to a terminal CO (such as model **12**), led to vibrational coupling of the C≡O and Fe-H stretches and introduced ν(CO) splittings that do not correspond to our Lo-3 experimental observations.

With the current DFT calculations, the FeMo-cofactor protonation scheme and the identity of the interstitial **X** (= $C^{4-}/N^{3-}/O^{2-}$) ligand were both found to be important for reproducing the Hi-3 and Lo-3 FT-IR spectra. The interplay of these alternatives in defining the charge state of the FeMo-cofactor model was stressed earlier, for example in connection to Mössbauer isomer shifts[27, 30] and redox potential[27, 30b, 31] calculations. For our $1e^-$ reduced Hi-3 and Lo-3 FeMo-cofactor states, we found single protonation of the cofactor at the μ^2 S2B sulfur optimal for the $\mathbf{X} = N^{3-}$ alternative, while double protonation at μ^2 S2B and μ^2 S5A gave the best results for $\mathbf{X} = C^{4-}$. The $\mathbf{X} = N^{3-}$ option provides very good correspondence (≤2 cm^{-1} offset) to the Hi-3 and Lo-3 signatures and allows to interpret the minor peaks of the mixed isotope experiment (see Figure 5), while the $\mathbf{X} = C^{4-}$ model

Author Manuscript Author Manuscript Author Manuscript Author Manuscript

results in somewhat larger frequency shifts of up to 8 cm^{-1} with respect to the FT-IR data (see Table S3 of the Supporting Material). However, since observed *vs.* computed frequency deviations of up to ~1% are inherent to the present DFT setup, our calculations cannot really discern whether **X** = N^{3-} or C^{4-}. We have no reason to doubt the **X** = C^{4-} assignment that derives from other methods.[2–3]

Before discussing how or whether the Hi-3/Lo-3 couple has a role in the inhibition of N_2 and other substrate reduction or perhaps in Fischer-Tropsch-like chemistry, we need to determine, in the nomenclature used by Hoffmann and coworkers,[28b, 32] its 'electron inventory'. This refers to the number of electrons delivered from the Fe protein (called *n*) to form the Hi-3 species, starting from the resting state called E_0. The equation $n = s + m - p$ takes into account the number of electrons transferred to substrate (*s*), the number delivered to the FeMo-cofactor metals (*m*), and the number of electrons transferred from the P-cluster (*p*). The EPR silence of the Hi-3 species implies that *n* is odd, in order to produce an even-electron (most likely $S = 0$) Hi-3 species from the $S = 3/2$ EPR-active odd-electron resting ($n = 0$) state. The fact that Hi-3 is stable for days or longer argues against a highly reduced species with $n \geq 3$, because such a species would presumably relax by H_2 evolution. Given the preference of CO for reduced metal ions, chemical intuition also argues against a more oxidized form of the FeMo-cofactor (hence negative values for *n*). We are left with $n = 1$, a $1e^-$ reduced FeMo-cofactor compared to resting MoFe protein. There is no evidence for P-cluster oxidation under these conditions, thus $p = 0$. Because the bound CO has not been reduced, $s = 0$. We thus get $m = n = 1$ for the FeMo-cofactor metal ion core electron count beyond the resting state.

A recent proposal suggests that the metal core of the FeMo-cofactor has only two accessible oxidation levels, the EPR-active resting state (M^N) with $m = 0$ and the one-electron-reduced EPR-silent state (M^R) with $m = 1$.[32] If so, then our Hi-3 species would retain the single electron on the FeMo-cofactor and be EPR-silent, whereas the lo-CO, hi-CO, and hi(5)-CO species, being *more* reduced than the resting state by an even number of electrons, would be EPR-active and these 'extra' electrons would be forced to reside on 'substrates'. Thus, the lo-CO, hi-CO and hi(5)-CO EPR signals would come from forms of N_2ase with $m = 0$ and $s = 2$ for a total of $n = 2$. The substrate-localized electrons could reside on either a formyl species or an as yet undetected hydride species. Partially reduced substrates are of course critical intermediates for C-C coupling reactions[33] as demonstrated previously by the formation of a similar range of hydrocarbons from N_2ase-catalyzed isocyanide reduction.[34]

Is the Hi-3 (or Lo-3) species relevant to N_2ase Fischer-Tropsch chemistry? Most mechanisms for Fe-catalyzed Fischer-Tropsch chemistry posit the presence of CO-derived reactants on adjacent Fe atoms,[35] and for N_2ase, intermediates with adjacent CO or $CH_xO_{0,1}$ species[7, 33] have also been proposed. Evidence for multiple binding sites in N_2ase dates back 40 years or more,[4b] but it has always been difficult to separate physically distinct binding sites on the same species from those produced by different redox levels and/or protonation states of the FeMo-cofactor. The current study is the first to demonstrate simultaneous terminal CO binding to distinct and adjacent Fe sites on the FeMo-cofactor. It thus demonstrates that two CO molecules can bind to Fe atoms only ~2.7 Å apart.

Author Manuscript Author Manuscript Author Manuscript Author Manuscript

Yang *et al.* observed that the α-H195Q. α-V70A *Av1* double mutant was much less efficient at hydrocarbon production than the α-V70A single mutant, and they suggested that α-H195 functions to deliver protons for the reduction of CO.[7, 36] Disruption of this proton transfer may also explain why we see a larger fraction of the Hi-3 species in the α-H195Q *Av1* compared to wild-type enzyme.[15] Additional work is of course needed to determine whether Hi-3 represents a requisite intermediate or a side reaction resulting from a 'proton bottleneck'.

Finally, the Hi-3 species is only 1-electron reduced from the resting state of the enzyme. Since the reduction of two CO molecules to C_2H_4 and 2 H_2O requires 8 electrons and 8 protons, there is a good deal of chemistry required between Hi-3 and the major product observed during CO reduction. Efforts to identify and characterize those additional species are of course in progress.

Experimental Section

Sample Preparation

Purified α-H195Q MoFe protein and Fe protein had specific activities of 2000–2800 nmol of H_2 (min/mg protein) $^{-1}$ and 2000–2300 nmol of H_2 (min/mg protein) $^{-1}$ respectively. The purified component proteins were exchanged into D_2O buffer containing 25 mM HEPES, pH 7.4, 10 mM $MgCl_2$, 250 mM NaCl. For preparation of CO-inhibited samples, low electron-flux conditions were obtained using a 1:4 molar ratio of Fe protein:MoFe protein. The reaction-mixture components, which consisted of 2.5 mM ATP, 5 mM $MgCl_2$, 30 mM creatine phosphate, 25 units/mL of creatine phosphokinase in 25 mM HEPES, pH 7.4 and 20 mM sodium dithionite were prepared in D_2O. Turnover was accomplished under 101 kPa CO. The reaction was quenched by the addition of ethylene glycol to a final concentration of 40% after 15 minutes. The resulting turnover product was concentrated in an Amicon microfiltration pressure concentrator using a regenerated cellulose PLHK ultrafiltration membrane with a 100,000 molecular weight cut off under 202 kPa CO of the same composition used for the turnover reaction.

Photolysis and FT-IR spectroscopy

The sample photolysis was conducted in an Oxford liquid He flow cryostat using a Sutter Instruments 300 W Lambda LS xenon arc lamp. Spectra were recorded at 4 cm^{-1} resolution with a Bruker V-70v FT-IR spectrometer and a MCT detector. For photolysis, the lamp was shone through the side of the cryostat oriented 90° to the IR light path. The sample was held at 45° to both beams. This allowed the use of quartz windows for the visible light. For wavelength dependent photolysis, we used a set of VersaChrome® tunable bandpass filters (Semrock) with central wavelengths at 340, 380, 410, 440, 470, 510, 550, 610, 700 and 800 nm.

DFT

The DFT calculations were done using the PBE functional and the LACV3P** basis set, as implemented in JAGUAR 7.7 software. For the first- and second-row elements, LACV3P** implies a 6-311G** triple-zeta basis set including polarization function. For the Fe and Mo

Author Manuscript Author Manuscript Author Manuscript Author Manuscript

atoms, LACV3P** uses the Los Alamos effective core potential (ECP), and the valence part is essentially of triple-zeta quality. The geometries optimized at the PBE/LACV3P** level were used for the analytic Hessian calculations, resulting in the harmonic frequencies and IR intensities discussed in the text. The analysis of the computed vibrational normal modes has been facilitated using an in-house Q-SPECTOR Python tool, applied to model the FT-IR spectra and assess the FeMo-cofactor bound CO modes via kinetic energy distribution (KED) approach. Further important details are given in the Supporting Information sections.

Supplementary Material

Refer to Web version on PubMed Central for supplementary material.

Acknowledgments

This work was funded by NIH GM-65440 (SPC), NSF CHE-0745353 (SPC), the DOE Office of Biological and Environmental Research (SPC), the Alexander von Humboldt Foundation (VP), and UniCat Cluster of Excellence (VP).

References

1. a) Peters JW, Szilagyi RK. Curr Opin Chem Biol. 2006; 10:101–108. [PubMed: 16510305] b) Barney BM, Lee H-I, Santos PCD, Hoffman BM, Dean DR, Seefeldt LC. Dalton Trans. 2006:2277–2284. [PubMed: 16688314] c) Dance I. Chem Asian J. 2007; 2:936–946. [PubMed: 17614310] d) Howard JB, Rees DC. Proc Natl Acad Sci USA. 2006; 103:17088–17093. [PubMed: 17088547]
2. Spatzal T, Aksoyoglu M, Zhang L, Andrade SLA, Schleicher E, Weber S, Rees DC, Einsle O. Science. 2011; 334:940. [PubMed: 22096190]
3. Lancaster KM, Roemelt M, Ettenhuber P, Hu YL, Ribbe MW, Neese F, Bergmann U, DeBeer S. Science. 2011; 334:974–977. [PubMed: 22096198]
4. a) Lind CJ, Wilson PW. J Am Chem Soc. 1941; 63:3511–3514.b) Hwang JC, Chen CH, Burris RH. Biochim Biophys Acta. 1973; 292:256–270. [PubMed: 4705133] c) Tolland JD, Thorneley RNF. Biochemistry. 2005; 44:9520–9527. [PubMed: 15996106]
5. a) Lee CC, Hu Y, Ribbe MW. Science. 2010; 329:642. [PubMed: 20689010] b) Lee CC, Hu YL, Ribbe MW. Angew Chem. 2011; 50:5545–5547. [PubMed: 21538750]
6. Hu Y, Lee CC, Ribbe MW. Science. 2011; 333:753–755. [PubMed: 21817053]
7. Yang Z-Y, Dean DR, Seefeldt LC. J Biol Chem. 2011; 286:19417–19421. [PubMed: 21454640]
8. Gerlach DL, Lehnert N. Ang Chem Int Ed. 2011; 50:7984–7986.
9. a) Pollock RC, Lee HI, Cameron LM, Derose VJ, Hales BJ, Orme-Johnson WH, Hoffman BM. J Am Chem Soc. 1995; 117:8686–8687.b) Christie PD, Lee HI, Cameron LM, Hales BJ, Orme-Johnson WH, Hoffman BM. J Am Chem Soc. 1996; 118:8707–8709.
10. Lee H-I, Cameron LM, Hales BJ, Hoffman BM. J Am Chem Soc. 1997; 119:10121–10126.
11. a) Lowe DJ, Eady RR, Thorneley RNF. Biochem J. 1978; 173:277–290. [PubMed: 210766] b) Davis LC, Henzl MT, Burris RH, Orme-Johnson WH. Biochemistry. 1979; 18:4860–4869. [PubMed: 228701] c) Cameron LM, Hales BJ. Biochemistry. 1998; 37:9449–9456. [PubMed: 9649328] d) Sørlie M, Christiansen J, Lemon BJ, Peters JW, Dean DR, Hales BJ. Biochemistry. 2001; 40:1540–1549. [PubMed: 11327812]
12. a) Moore VG, Tittsworth RC, Hales BJ. J Am Chem Soc. 1994; 116:12101–12102.b) Maskos Z, Fisher K, Sørlie M, Newton WE, Hales BJ. J Biol Inorg Chem. 2005; 10:394–406. [PubMed: 15887041]
13. a) George SJ, Ashby GA, Wharton CW, Thorneley RNF. J Am Chem Soc. 1997; 119:6450–6451.b) Thorneley, RNF.; Ashby, GA.; George, SJ. Nitrogen Fixation: From Molecules to Crop Productivity. Pedrosa, FO.; Hungria, M.; Yates, G.; Newton, WE., editors. Kluwer; The

Author Manuscript Author Manuscript Author Manuscript Author Manuscript

Netherlands: 2000. p. 39-40.c) Yang Z-Y, Seefeldt LC, Dean DR, Cramer SP, George SJ. Angew Chem. 2011; 123:286–289.

14. Pickett CJ, Vincent KA, Ibrahim SK, Gormal CA, Smith BE, Best SP. Chem Eur J. 2003; 9:76–87. [PubMed: 12506366]
15. Yan L, Dapper CH, George SJ, Wang HX, Mitra D, Dong WB, Newton WE, Cramer SP. Eur J Inorg Chem. 2011:2064–2074.
16. Ansari A, Berendzen J, Braunstein D, Cowen BR, Frauenfelder H, Hong MK, Iben IET, Johnson JB, Ormos P, Sauke TB, Scholl R, Schulte A, Steinbach PJ, Vittitow J, Young RD. Biophys Chem. 1987; 26:337–355. [PubMed: 3607234]
17. Myers WK, Dong W, Dapper CH, Yan L, Scott A, George SJ, Britt D, Newton WE, Cramer SP. in preparation. 2012
18. Bagley KA, Vangarderen CJ, Chen M, Duin EC, Albracht SPJ, Woodruff WH. Biochemistry. 1994; 33:9229–9236. [PubMed: 8049224]
19. Austin RH, Beeson KW, Eisenstein L, Frauenfelder H, Gunsalus IC. Biochemistry. 1975; 14:5355–5373. [PubMed: 1191643]
20. Darensbourg DJ. Inorg Chem. 1972; 11:1606–1609.
21. Maskos Z, Hales BJ. J Inorg Biochem. 2003; 93:11–17. [PubMed: 12538048]
22. Sarma R, Barney BM, Keable S, Dean DR, Seefeldt LC, Peters JW. J Inorg Biochem. 2010; 104:385–389. [PubMed: 20022118]
23. Einsle O, Tezcan FA, Andrade SLA, Schmid B, Yoshida M, Howard JB, Rees DC. Science. 2002; 297:1696–1700. [PubMed: 12215645]
24. Dance I. Dalton Trans. 2011; 40:6480–6489. [PubMed: 21584340]
25. Durrant MC. Biochemistry. 2004; 43:6030–6042. [PubMed: 15147187]
26. a) Xiao Y, Fisher K, Smith MC, Newton W, Case DA, George SJ, Wang H, Sturhahn W, Alp EE, Zhao J, Yoda Y, Cramer SP. J Am Chem Soc. 2006; 128:7608–7612. [PubMed: 16756317] b) Lukoyanov D, Pelmenschikov V, Maeser N, Laryukhin M, Yang TC, Noodleman L, Dean DR, Case DA, Seefeldt LC, Hoffman BM. Inorg Chem. 2007:46, 11437–11449.c) Pelmenschikov V, Case DA, Noodleman L. Inorg Chem. 2008; 47:6162–6172. [PubMed: 18578487]
27. Harris TV, Szilagyi RK. Inorg Chem. 2011; 50:4811–4824. [PubMed: 21545160]
28. a) Lee HI, Hales BJ, Hoffman BM. J Am Chem Soc. 1997; 119:11395–11400.b) Lee HI, Sørlie M, Christiansen J, Yang TC, Shao JL, Dean DR, Hales BJ, Hoffman BM. J Am Chem Soc. 2005; 127:15880–15890. [PubMed: 16277531]
29. Alben JO, Beece D, Bowne SF, Doster W, Eisenstein L, Frauenfelder H, Good D, McDonald JD, Marden MC, Moh PP, Reinisch L, Reynolds AH, Shyamsunder E, Yue KT. Proc Natl Acad Sci USA. 1982; 79:3744–3748. [PubMed: 6954517]
30. a) Vrajmasu VV, Bominaar EL, Münck E. Inorg Chem. 2003; 42:5974–5988. [PubMed: 12971768] b) Lovell T, Liu T, Case DA, Noodleman L. J Am Chem Soc. 2003:125, 8377–8383.
31. Dance I. Inorg Chem. 2006; 45:5084–5091. [PubMed: 16780330]
32. Doan PE, Telser J, Barney BM, Igarashi RY, Dean DR, Seefeldt LC, Hoffman BM. J Am Chem Soc. 2011; 133:17329–17340. [PubMed: 21980917]
33. Dance I. Dalton Trans. 2011; 40:5516–5527. [PubMed: 21487574]
34. Kelly M. Biochem J. 1968; 107:1–6. [PubMed: 5642620]
35. de Smit E, Weckhuysen BM. Chem Soc Rev. 2008; 37:2758–2781. [PubMed: 19020686]
36. Fisher K, Dilworth MJ, Newton WE. Biochemistry. 2000; 39:15570–15577. [PubMed: 11112544]

Author Manuscript Author Manuscript Author Manuscript Author Manuscript

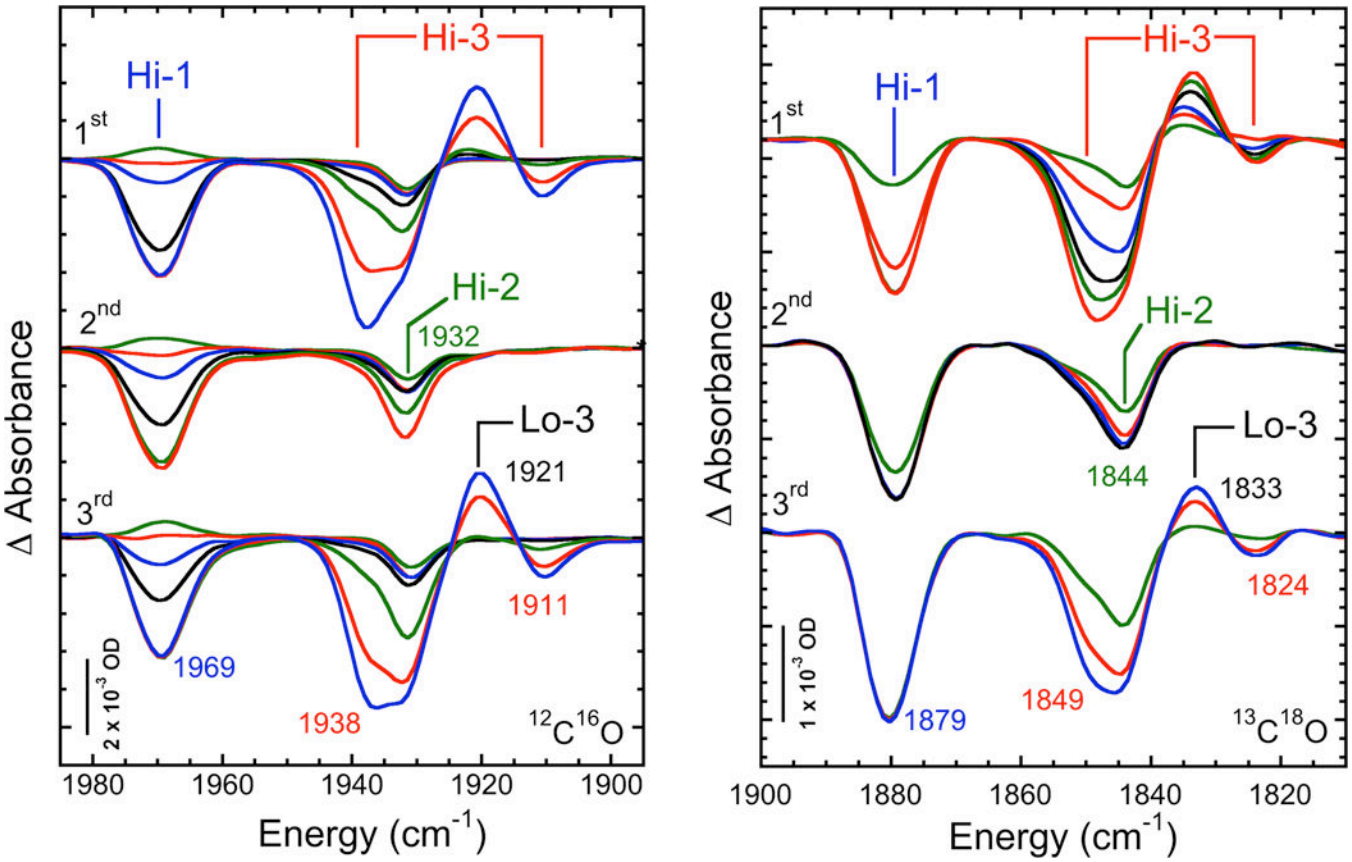

Figure 1.

Time dependent absorbance changes upon photolysis at 4 K and thermal cycling of CO-inhibited α-H195Q N_2ase in D_2O-based 25 mM HEPES, pH 7.4 buffer with 40% ethylene glycol. Left: 'hi-$^{12}C^{16}O$' conditions. Top to bottom: 1st photolysis, time points shown are 0.5, 4, 9, 52s, 3, 30, 150 min; 2nd photolysis, after warming to 120 K for 20 min, time points shown are 0.5, 7, 13, 35s, 2, 30min; 3rd photolysis after poising at ~263 K for 16 h, time points shown are 0.5, 5, 13, 30s, 5, 70, 270 min. Right: 'hi-$^{13}C^{18}O$' conditions. Top to bottom: 1st photolysis, time points shown are: 0.5, 2, 10, 31, 60, and 122 min; 2nd photolysis, after warming sample to 120 K for 10 min, time points shown are: 2, 10, 30, and 60 min; 3rd photolysis, after warming sample to 233 K for 8 h, time points shown are: 3, 23, and 63 min.

Author Manuscript Author Manuscript Author Manuscript Author Manuscript

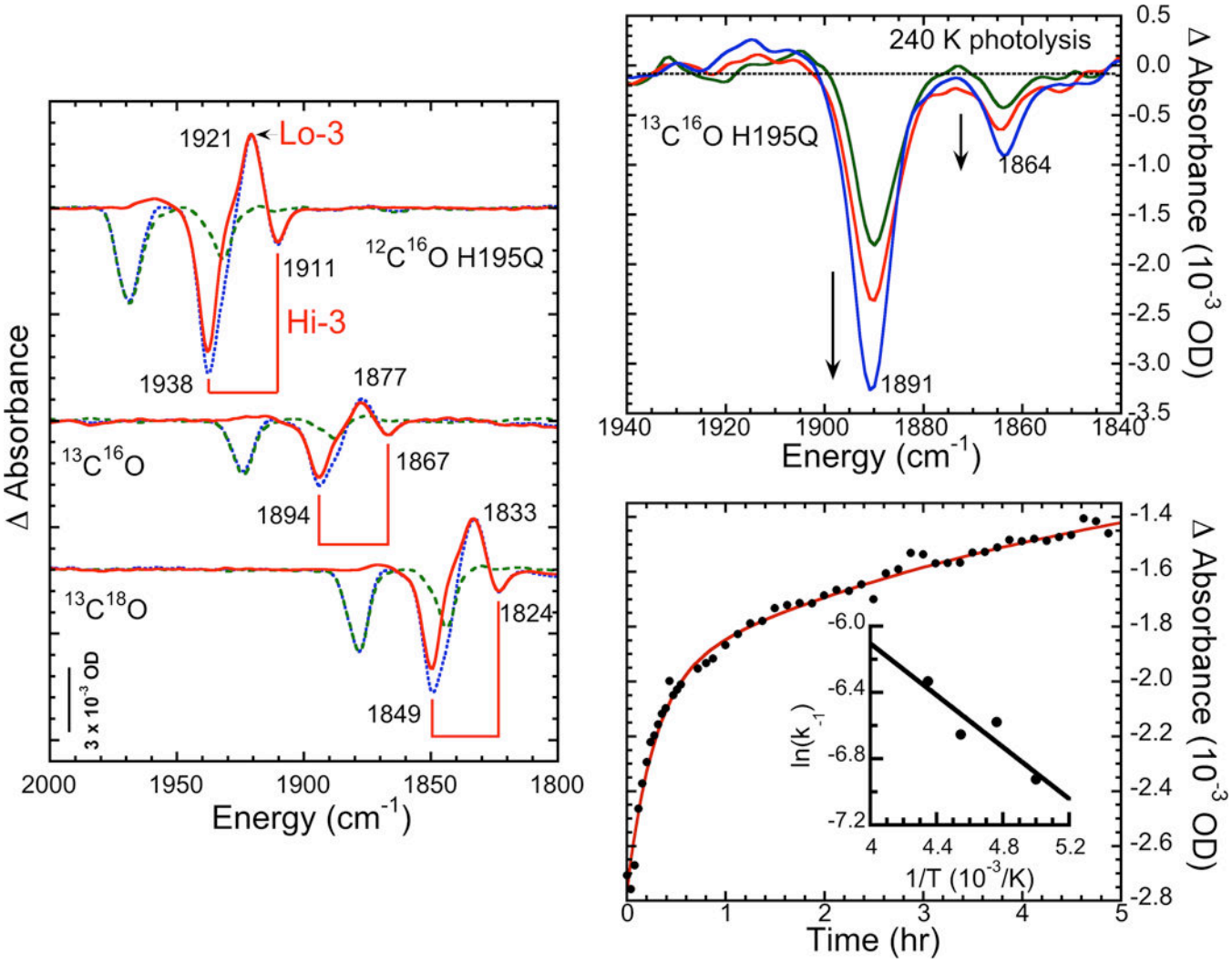

Figure 2.

Left: extraction of Hi-3/Lo-3 spectra (—) by subtraction of 2nd photolysis spectra (- -) (photolyzed at 4K after recombination at 120 K) from 1st spectra (- -). Top right: photolysis at 240 K. Times are 40 (—), 60 (—), and 150 (—) min. Bottom right: recombination data for 210 K, fit with dual exponential. Inset: Arrhenius plot for fast phase of recombination, yielding activation energy of 6.5 kJ mol^{-1}.

Author Manuscript Author Manuscript Author Manuscript Author Manuscript

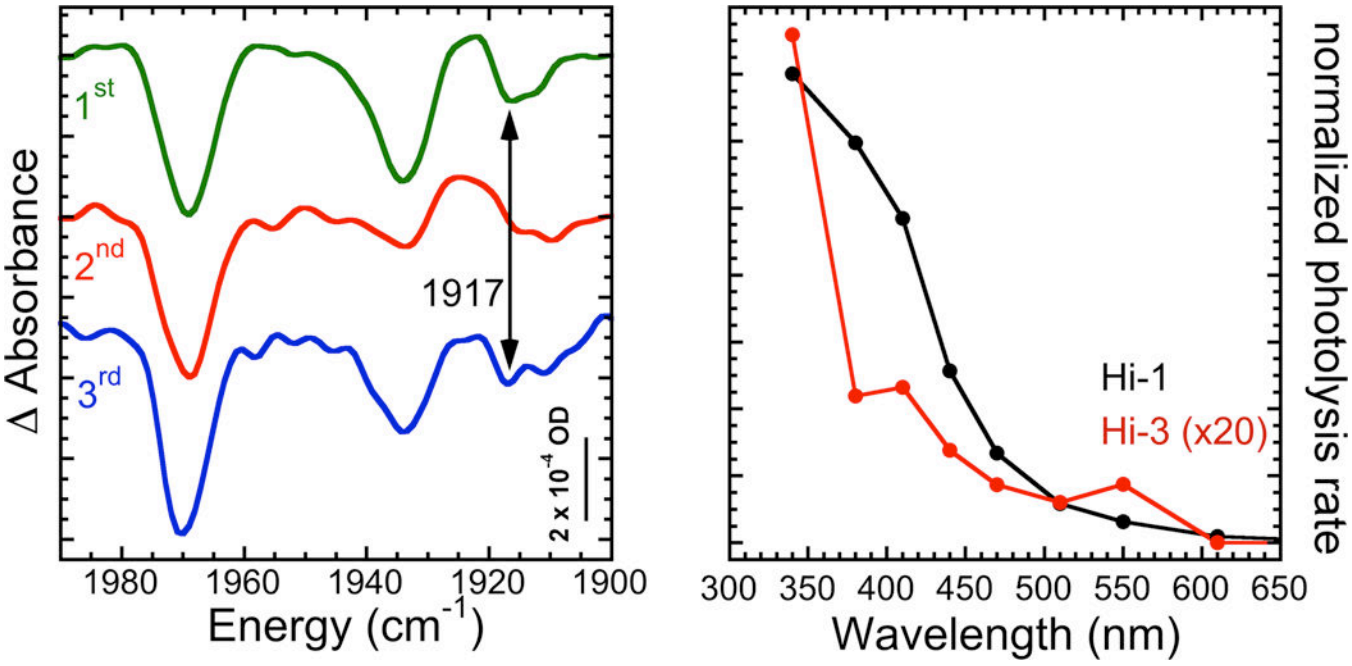

Figure 3.

Left: Mixed isotope effects on CO-inhibited N_2ase. Top to bottom: 1st photolysis for 122 min; 2nd photolysis for 60 min, after warming to 120 K for 10 min; 3rd photolysis for 63 min, after warming to 233 K for 8 h. Right: wavelength dependence of Hi-3 photolysis *vs*. Hi-1 photolysis.

Author Manuscript Author Manuscript Author Manuscript Author Manuscript

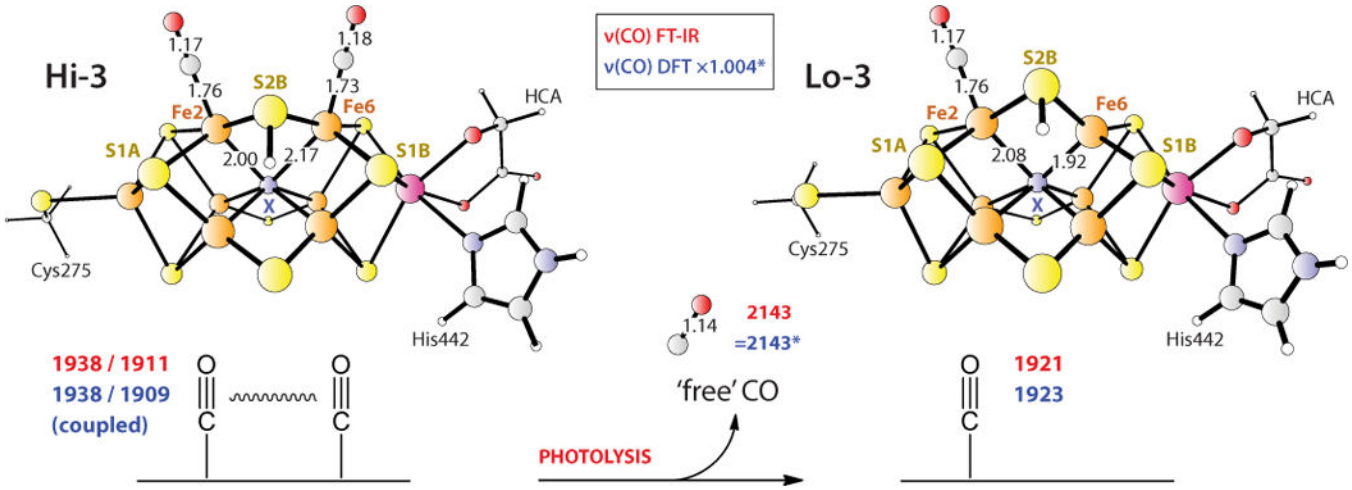

Figure 4.

Favored DFT-optimized Hi-3 and Lo-3 structures. The observed FT-IR (red) and calculated DFT (blue) frequencies (cm^{-1}) are given for the $X = N^{3-}$ models. Selected interatomic distances (Å) are shown. Similar results were obtained with the now-favored $X = C^{4-}$ assignment, provided S5A was also protonated (see text). The asterisk implies DFT frequency scaling as described in Methods. For the model coordinates and animated vibrational modes, see the Supporting Material section.

Author Manuscript Author Manuscript Author Manuscript Author Manuscript

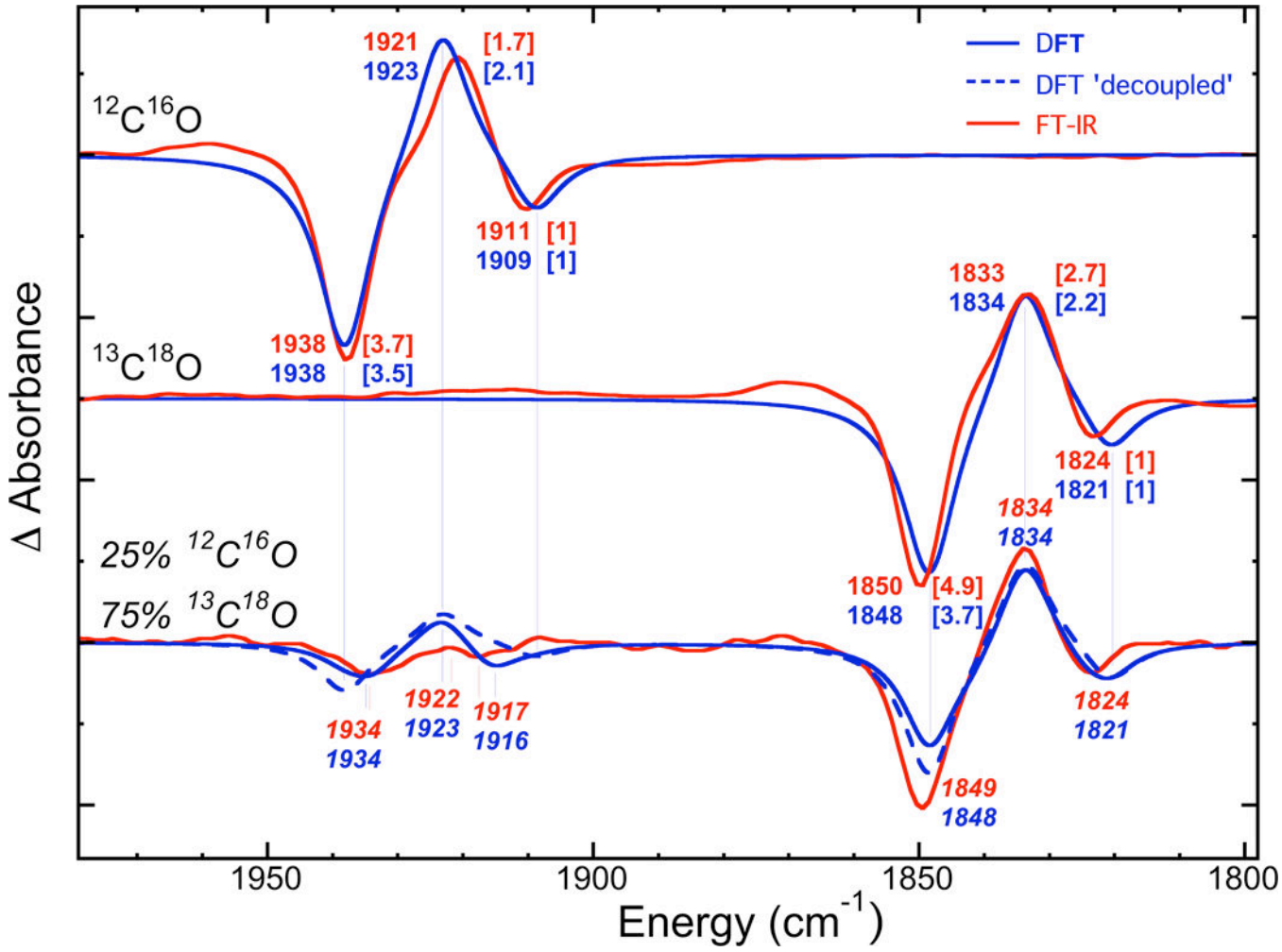

Figure 5.

Overlay of the FT-IR (red) vs. DFT (blue) modelling (blue) of the Hi-3→Lo-3 photolysis difference spectra for pure 12C16O (top) and 13C18O (middle), and the mixed 25% 12C16O / 75% 13C18O (bottom) isotope experiments. The observed FT-IR and calculated DFT frequencies are in cm^{-1}; the wave numbers for the mixed isotope case are in italic for clarity. For pure isotope spectra, the peak intensities are given in square brackets relatively to the lower frequency Hi-3 band. The simulation of the hypothetical 'decoupled' mixed isotope spectrum is presented as the broken line; the long vertical lines imply that this spectrum provides no peak shifts with respect to the pure isotope spectra.